ACS APPLIED NANO MATERIALS

www.acsanm.org
Article

Nanoweb for Nanobugs: Nanofiber Filter Media for Face Masks

Katarina E. Goodge,* Wendy A. Alwala, and Margaret W. Frey

Cite This: ACS Appl. Nano Mater. 2024, 7, 6120–6129
Read Online

ABSTRACT: Nonwoven face masks are being explored as potential multifunctional, wearable, and smart healthcare devices. The fibers in the nonwoven layers can effectively mechanically and electrostatically capture submicrometer particles depending on their fiber size, porosity, and surface charge. While surface charge enhances the filtration of mechanical capture alone, charge is sensitive to moisture, heat, disinfectant solvents, and storage. TriboElectric NanoGenerators (TENG) are a solution to leverage the biomechanical action of respiration to generate a skin-safe level of charge to maintain the electrostatic capture mechanism throughout the wear cycle. In this study, hexadimethrine bromide (PB) and poly(methyl vinyl ether-*alt*-maleic anhydride) (PMA) were mixed with poly(vinyl alcohol) (PVA) and electrospun into hybrid PVA nanofibers to compare their filtration performance to pure PVA nanofibers. Fiber and pore size were measured from scanning electron microscopy (SEM) images, fiber chemistry was characterized via Fourier Transform InfraRed (FTIR) spectroscopy, TENG performance was measured via output voltage, static and dynamic breathability were measured via Air Permeability (AP) and in-line differential pressure (dP), respectively, and filtration efficiency (FE) was calculated from penetrated particle count during a simulated breathing experiment. Optimized for fiber and pore size distributions, PVA fibers achieved 92.3% FE of 0.3 μm particles and dP of 53.8 cm water, PVA/PB fibers achieved 92.5% FE and 18.3 cm water, and PVA/PMA fibers achieved 88.0% and 66.1 cm water. Output voltage was found to be dependent on moisture content, with the pure PVA nanofibers generating the highest positive voltage when wet, PVA/PMA nanofibers generating a less positive voltage, and PVA/PB generating a negative voltage. The combination of filtration and TENG performance positions both the pure and hybrid PVA nanofibers for incorporation into a face mask as multifunctional nanofiber layers. The hybrid PVA nanofibers specifically can be further tested as selective capture membranes toward controlled adhesion, on-mask sample collection/preparation, pathogen detection, and health data monitoring.

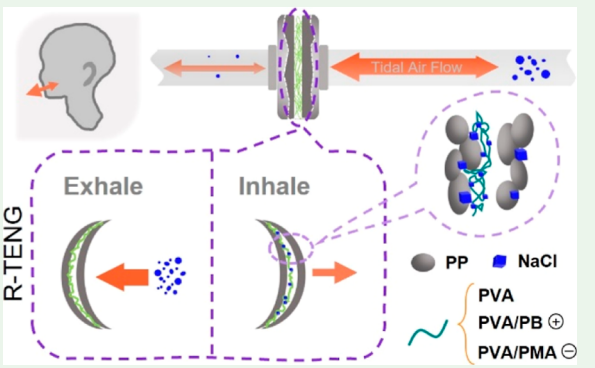

KEYWORDS: *electrospinning, nanofibers, face mask, filtration, simulated breathing, aerosol, cloth mask*

1. INTRODUCTION

Personal air filtration devices such as half-face respirators, surgical masks, and nonmedical cloth face coverings have differing levels of respiratory protection and source control. For infectious diseases, the primary challenge is capturing the submicrometer-sized pathogens or "nanobugs". While N95 respirators in particular exhibit greater than 95% filtration efficiency (FE) of 0.3 μm particles owing to their electret charge, this electret charge accumulation on the microfiber surface is only semidurable and can dissipate with storage time,[1] repeat use,[2] high humidity,[3−5] heat,[4,5] and disinfectant solvent.[6−8] Nanofibers have theoretically and experimentally been shown to collect greater than 95% of submicrometer particles with mechanical capture mechanisms alone (interception, inertial impaction, diffusion, and gravitational settling), allowing for storage-stable, reusable, and highly breathable core filter layers.[7,9]

The theory of particle capture on fibrous filters is well developed, and the predicted relationships between fiber diameters, FE, and differential pressure (dP) across the filter have been confirmed experimentally to be strong functions of fiber size, particle size, filter porosity, filter thickness, and face velocity. Briefly, minimum total FE occurs between 100 and 500 nm, the most penetrating particle size (MPPS), where particles are too large for diffusion to be effective but too small for interception or impaction. FE at MPPS increases while the particle size of MPPS decreases as fiber diameter decreases. As the fiber diameter approaches the gas mean path, the "no-slip" boundary condition of Stoke's law no longer holds, and the "slip" at the fiber surface becomes significant at diameters <1 μm.[10] For an effective face mask, filter layers must efficiently prevent particles from penetrating while also remaining mechanically stable. Prefilter substrates capture larger droplets

Received: December 14, 2023
Revised: February 20, 2024
Accepted: February 23, 2024
Published: March 6, 2024

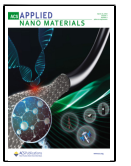

(<5 μm) and provide mechanical support to core filter layers. Nanofiber webs provide highly efficient mechanical capture of particles but are inherently very fragile. The thinner the fiber diameter, the weaker the fiber; so, an optimal nanofiber web will have the largest possible fibers where the slip-flow regime exists. Weak fibers can break off and be carried with the airflow stream, which can reduce the filtration efficiency, endanger the user by inhaling the nanosized fiber fragments, and pollute the environment if it successfully permeates the inner or outer mask layers. While larger fibers are stronger, they have a smaller specific surface area and reduced adsorption capacity. Thinner fibers also create smaller pores, which increase the tortuosity of the web for enhanced particle capture but simultaneously reduce the air permeability. Therefore, a balance can be found between higher FE performance of smaller fibers and higher strength and breathability of larger fibers.

Surpassing mechanical filtration, electrostatically charged electret fibers had high initial FE, but due to the electrical double layer or high relative humidity from exhaled breath or ambient air conditions, the charged filters lost apparent charge, and therefore FE, as particles are captured.[3,11,12] An alternative method for enhancing the overall FE with electrostatic capture on nanofiber filters is via TriboElectric NanoGenerators (TENGs), which convert mechanical energy into electricity. Filter media constructed with TENGs have been shown to regenerate the lost surface charge by harnessing charges generated from the friction of multiple fabric layers shifting from the cyclic air flow of breathing (driven by respiration, R-TENG); however, they are sensitive to humidity.[13−15] The electrical output from a TENG is dependent on the ability of materials comprising the TENG to acquire a positive or negative charge and the relative strength of those charges. A recent study showed that the electrical output and open circuit voltage of poly(vinyl alcohol) (PVA) (+)−polypropylene (PP) (−) TENG increased with increasing humidity, while both electrical output and open circuit voltage decreased with increase in humidity for an aluminum (+)−PP (−) TENG, an otherwise promising triboelectric material combination.[16] Wang and colleagues showed that the humidity amplification of the TENG performance of the PVA−PP was attributed to the hydrogen bonding of water with PVA; the water molecules were immobilized onto the nanofiber surface and participated in the triboelectric charging. They further showed that PVA electrospun nanofibers exhibited higher charge storage performance (slower charge dissipation rate) compared to commercial medical PP masks and could regain triboelectric charge by simply tapping the PVA-based mask without doffing it.[12] Therefore, TENG assemblies show promise in supplying electrostatic charge to sustain high FE.

Beyond basic filtration, high performance nanofiber filters have since been further enhanced by integrating other functionalities through design and material development toward a new paradigm of smart protective devices. Face mask studies that emerged from the COVID-19 pandemic leveraged this size effect for nanofibers alongside the low basis weight, large surface area to volume ratio, and high porosity for use as multifunctional fabric systems within face masks.[17−19] Depending on the fiber material composition or surface modification, face masks can serve advanced functions such as antimicrobial, fluid-resistant, reusable, environmentally sustainable material use and disposal, pathogenic detection, and health data monitoring smart devices.[20−23] Hexadimethrine bromide (PB) and poly(methyl vinyl ether-*alt*-maleic anhydride) (PMA) are cationic and anionic polymers, respectively, that have previously been electrospun with PVA for use as selective capture membranes in liquid filtration and microfluidic analytical systems.[24−27] This study extends the application of these polyionic nanofibers to air filtration, where the liquid−solid interface is localized to each aerosol droplet and fiber surface. PB and PMA when mixed with PVA can influence the strength of the positive or negative charges that are generated in the R-TENG assembly, serving as both FE enhancement and potential selective capture diagnostic nanofiber webs.

Herein, a self-charging (TENG) and humidity-resistant nanofiber−microfiber hybrid filter media is established to maintain filtration performance over 30 min of simulated breathing even with moisture accumulation. PVA/ionomer blend nanofibers were electrospun without use of any potentially hazardous solvents onto a lightweight, polypropylene (PP) spunbond substrate and characterized for use as the core filter layer in a face mask configuration. Nanofiber and pore size contributions to mechanical filtration, surface available ionic charges from ionomer addition, and electrical charge from TENG formation were studied for their overall effect on FE, dP, and moisture accumulation. For the output voltage measurement, the TENG assembly of a nanofiber layer sandwiched between two layers of microfiber substrate was positioned between two copper electrodes, and finger tapping was used to mimic biomechanical contact separation or respiration mode. Polydisperse, aqueous sodium chloride aerosol was used as a model aerosol in a simulated breathing apparatus that mimics the tidal breathing of adults. Differential pressure was monitored across the filter, and particle counts for 0.3, 0.5, and 1.0 μm particles were converted to filtration efficiency. At neutral pH, the nanofiber size had a larger size effect than the nanofiber electron donor/acceptor character. These hybrid PVA nanofibers coupled with conventional PP nonwoven show promise for prolonged face mask use with facile fabrication, low add-on, high breathability, tunable surface adhesion, biomechanical charge retention, and sustained filtration performance. The inclusion of PMA and PB in the formation of PVA nanofibers did not affect the filtration performance of the PVA. Therefore, these surface-active nanofibers can be used for further functionalization as a multifunctional wearable smart device.

2. EXPERIMENTAL SECTION

2.1. Materials. Poly(vinyl alcohol) (PVA) (M_W = 78 kDa, 99.7% hydrolyzed) was purchased from Polysciences, Inc., Warrington, PA, USA. Hexadimethrine bromide (polybrene, PB) (M_W = 4−6 kDa), poly(methyl vinyl ether-*alt*-maleic anhydride) (PMA) (M_W = 216 kDa), and Triton X-100 (p-tertiary-octylphenoxy polyethyl alcohol), as shown in Figure 1, were purchased from Sigma-Aldrich, St. Louis, MO, USA. A polypropylene (PP) spunbond substrate was purchased from JoAnn Stores Inc. All the materials were used as received. Deionized (DI) water was used as a solvent to prepare the PVA spinning dope.

2.2. Fabrication of Electrospun Nanofibers. Fabrication of the hybrid PVA nanofiber webs was based on previous studies.[24−27] PVA and PMA were dissolved in separate DI water solutions in an oven at 95 °C for 3 and 2 h, respectively. PB was dissolved in DI water at room temperature. All concentrations and mass ratio of PVA to functional polymer (FP) are listed in Table 1. Two concentrations of PVA/PMA were prepared to obtain the desired variation in the fiber size. PVA was mixed with the corresponding functional polymer, and nonionic surfactant Triton X-100 was added to the spinning dope to

https://doi.org/10.1021/acsanm.3c06034
ACS Appl. Nano Mater. 2024, 7, 6120−6129

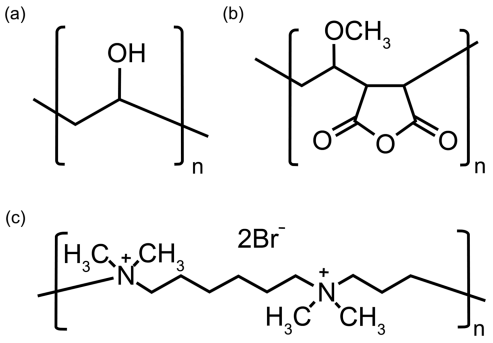

Figure 1. Chemical structure of (a) PVA, (b) PMA, and (c) PB polymers.

Table 1. Electrospinning Solution Parameters

sample	wt %	PVA/FP	charge
PVA	10		none
PVA/PB	10	70:30	cationic
PVA/PMA-10	10	70:30	anionic
PVA/PMA-14	14	70:30	anionic

reduce the surface tension of the water (X-100/DI-water = 0.5/99.5 w/w). Each solution was shaken overnight.

Each solution was added to separate 5 mL BD plastic syringes each with 21-gauge BD PrecisionGlide needle. A high voltage supply (Gamma High Voltage Research) provided 18 to 20 kV to the needle tip, and a grounded copper collector, placed 10 to 15 cm away, was covered with the PP nonwoven substrate. The solution feed rate was maintained between 0.5 and 1.0 mL/h using a programmable PHS Ultrasyringe pump (Harvard Apparatus). Electrospinning took place at 30% relative humidity in a Plexiglas humidity-control box (Plas Labs) for 30 to 60 min. See Table S1 for spin parameter details. The resulting nonwoven membranes were thermally treated at 120 °C in a convection oven for 24 h to remove residual solvent and increase the water stability of the nanofibers.

2.3. Characterization of Nanofibers. Fiber morphology and diameter were examined using scanning electron microscopy (Zeiss Gemini 500 SEM) with an accelerating voltage of 2 kV. Energy-dispersive X-ray spectroscopy (EDX) spectra were collected with an accelerating voltage of 10 kV and 120 μm aperture. Samples were sputter-coated with gold−palladium for SEM and EDX. ImageJ open-source software (National Institutes of Health) was used to measure the fiber diameters and pore Feret diameters.

The chemical structure was analyzed with attenuated total reflection-Fourier transform infrared (ATR-FTIR) spectroscopy (PerkinElmer Frontier). Each spectrum was an average of 64 scans obtained between 4000 and 600 cm^{-1} at a resolution of 4 cm^{-1}.

2.4. Performance of the Nanofiber/Substrate System. Air permeability (AP) of the nanofiber/substrate composite was measured following ASTM D737 using a sampling plate (ID = 1 in.) and a Frazier Low Differential Pressure Air Permeability Tester (Frazier Instrument Co.). AP values were scaled by a factor of 7.56, as shown in Figure S1, to compare to the sampling plate size (ID = 2.75″) of the recommended minimum AP of 37.5 $ft^3/min/ft^2$ in AATCC M14.

Triboelectric charge generation of a TENG assembly, as shown in Figure 2a, was characterized by measuring the output voltage with a sourcemeter (Keithley 2400) set to the measurement mode. The two layers of fabric (3 cm × 6 cm) were sandwiched between two copper plates (7.7 cm × 7.6 cm × 1.08 mm), each plate attached to an electrode probe. Each composite sample was tested in "dry" and "wet" conditions with simple periodic pressure (finger tapping of approximately one tap per second) applied to the top copper plate to simulate the exhaled breath airflow compressing and releasing the two layers of fabric. The dry condition was as prepared, and wet condition was after adding 0.8 mL NaCl solution (approximately 30 min of simulated breathing) dropwise onto the sample.

Particle capture was evaluated by using a simulated breathing apparatus, as shown in Figure 2b. Briefly, a respirator pump (Harvard Apparatus, Model #B-55172) was set to 200 mL tidal volume, 25 breaths/min, and 50/50 inspiration/expiration ratio. Aerosol was generated from 1 M NaCl aqueous solution by an air compressor (Medline Aeromist Plus Nebulizer Compressor, Model #MEDHCS60004). This nebulizer method generates fine aerosol particles (<5 μm) by the coarse spray droplets being removed from the exiting aerosol stream by impaction with nebulizer wall and drained back to the salt solution reservoir.[5] Samples were conditioned in the testing room at 50 ± 2% relative humidity and 20 ± 2 °C for minimum 24 h and cut into circles (d = 38 mm). The filter assembly consisted of the nanoweb/substrate as the filter layer and another PP nonwoven layer as the prefilter layer. The filter assembly was mounted into a filter holder downstream of the nebulizer bulb. Uncaptured salt aerosol traveled through an inline moisture filter (Whatman cellulose filter paper type 4) and was measured by a particle counter (MetOne Instruments, Aerocet 531S). High resolution channels on the particle counter were chosen as 0.3, 0.5, and 1.0 μm and scanned for 60 s increments with no hold. Each sample was run for 30 min, and each blank was run for 10 min, per cycle. FE (%) for each size channel was calculated using eq 1

$$\mathrm{FE}(t) = \frac{N_{\mathrm{blank}} - N_{\mathrm{sample}}(t)}{N_{\mathrm{blank}}} \quad (1)$$

where N_{sample} is the particle count at the corresponding size channel at a specified time with a sample in the filter holder, and N_{blank} is the average particle count without a sample in the filter holder. Samples were weighed before testing (W_i), directly after testing (W_w), and 24 h after testing (W_d). Pressure was monitored by a manometer (8205 Hand-held 5 psi Digital Differential Pressure).

2.5. Statistical Analysis. All electrospinning conditions were performed in triplicate. Where descriptive statistics are reported, the mean and standard error are given. Statistical analyses were performed in MATLAB (MathWorks).

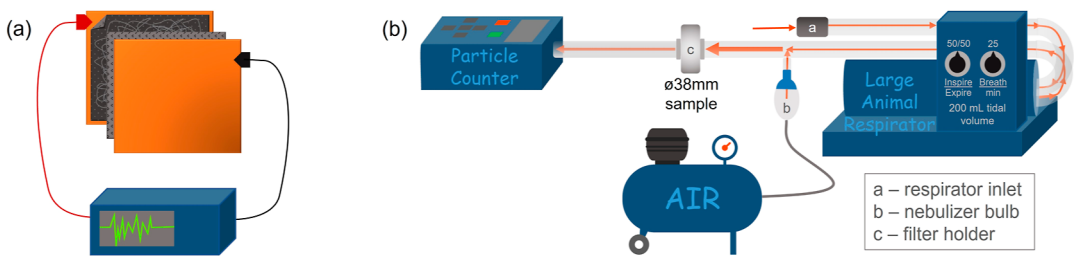

Figure 2. Schematic of (a) TENG assembly with copper bottom and top plates attached to negative and positive probes and PP nonwoven layers sandwiching the electrospun layer and (b) simulated breathing apparatus for flat filter testing.

https://doi.org/10.1021/acsanm.3c06034
ACS Appl. Nano Mater. 2024, 7, 6120−6129

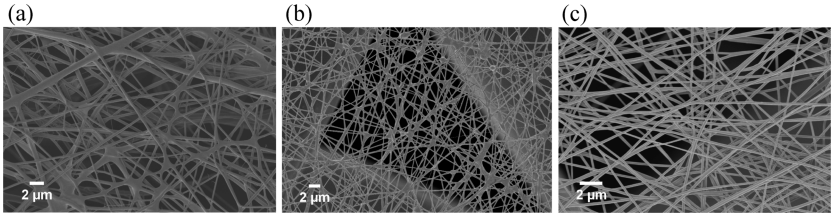

Figure 3. SEM images of heat-treated (a) PVA, (b) 70/30 PVA/PB, and (c) 70/30 PVA/PMA nanofiber webs at spin variation 3. See Figure S2 for spin variations 1−5.

3. RESULTS AND DISCUSSION

3.1. Nanofiber Web Characterization. *3.1.1. Fiber and Pore Morphology; Fiber and Pore Size.* PVA was electrospun alone and blended with PMA and PB at various spinning conditions onto PP microfiber nonwoven substrate and then thermally treated to improve water resistance of the nanofibers. SEM images of each polymer and spin condition in Figure 3 show that the morphology of PVA/PMA has less occurrence of bead formation than either neat PVA or PVA/PB. PVA spinning produced beading, splashing, and nanonets, consistent with previous studies reporting the difficulty of spinning pure PVA nanofibers.[24−26] PVA/PB blend shows beading and weld/fusion points at the intersection of fibers, suggesting the fibers did not dry completely before reaching the collector. As spin conditions were increased from 1 to 4, the beading and fiber fusion decreased as the solvent evaporated more completely prior to fiber collection. The positive charge on PB, with a positive applied voltage, could also contribute to the difficulty in forming uniform fibers. The negative charge on PMA had the opposite effect, with uniform, smooth fibers produced at all spin conditions and both 10 and 14 wt % concentrations.

Fiber sizes were measured with imageJ software, and the means ± standard error are reported in Table S2 (Supporting Information). Filtration efficiency is a strong function of fiber diameter; however, the samples' fiber diameters were only weakly related to spin condition as any fluctuations in electrospinning parameters, such as ambient relative humidity, can shift the fiber size distribution. Thus, samples were grouped by their fiber diameter instead of spin condition for subsequent filtration performance examination to elucidate the relationship between fiber properties and filter performance for face mask application. Diameter groups were determined by performing a one-way analysis of variance (ANOVA). The fiber diameter distributions were found to be either normal or log−normal. While the assumption for normality was not met, the sensitivity of the ANOVA test is minimally affected by moderate deviations from normality. A statistically significant difference was found in the sample means with $p < 0.05$. Therefore, a posthoc multiple comparisons analysis was performed to determine which pairs of means were statistically significantly different. Samples were grouped to minimize the number of groups of like-sized samples listed in Table 2 and Figure S3. Each polymer was sorted into size groups 155 to 258 nm for group A, 238 to 410 nm for group B, 407 to 570 nm for group C, and >792 nm for group D. Increased weight percent PVA/PMA-14 wt % was specifically included as PVA/PMA-10 diameter was invariant to variation in spin conditions and did not have representation in group C. An increase in concentration generally translates to an increase in fiber diameter, as was the case for PVA/PMA.

Table 2. Nanofiber Size Groups A−D with Their Corresponding Sample Content and Size Range

group	number of samples			mean fiber size range (nm)
	PVA	PVA/PB	PVA/PMA	
A		8	12	155−258
B	5		6	238−410
C	7	4	2	407−570
D	1			792

The nanofiber webs were spun for relatively short times, between 30 and 60 min, to thinly coat the substrate. Thus, thickness was not easily differentiable, and instead pore size was used as the measure for tortuosity. Reyes and Frey previously proved the correlation between mean pore diameter measured via imageJ analysis of SEM images and capillary flow porometry.[28] Here, the Feret diameters of sample pores and fiber diameters were measured with ImageJ. Figure 4 shows how similar fiber size distributions have variable pore size distributions. This polydispersity and differences in porosity (i.e., fiber density packing) contribute to significant differences in breathability and filtration performance.[29] See Figures S4 and S5 for ANOVA and Tukey posthoc results, respectively. Group A exhibited the narrowest fiber size distributions across polymer types with the other groups exhibiting wider distributions extending into neighboring groups (Figure S3). PVA/PMA group A samples had narrow fiber and pore size distributions with small means, whereas the larger fiber size groups tended to have larger pores. Thus, the thin fibers formed compact, tortuous webs, and the coarser fibers formed more open webs.[30]

3.1.2. Fiber Chemistry. The blend ratio of PVA to functional polymer and thermal treatment temperature were optimized in previous studies.[24,26] Exposure of negative charges on PMA occurs during the dissolution step of the electrospinning solution preparation; when in contact with aqueous solution above PMA's pK_a of 4.16, the maleic anhydride groups hydrolyze to carboxyl groups and further ionize to the carboxylate groups.[25,26] Undergoing thermal treatment, PVA will chemically cross-link with the maleic anhydride in PMA and physically cross-link via intermolecular hydrogen bonding with itself and PB, as shown in Figure 1. Successful thermal treatment increases the moisture resistance of the fibers without additional chemicals so that they do not swell when in contact with exhaled breath aerosol or dissolve in the accumulated moisture during the extent of filter use. The available surface charge is controlled by the number of unreacted maleic anhydride groups converted to carboxyl groups for PMA and number of surface-available quaternary ammonium cations for PB.

ATR-FTIR spectra of pure polymers and electrospun nanofibers in Figure 5 were used to confirm the presence of

https://doi.org/10.1021/acsanm.3c06034
ACS Appl. Nano Mater. 2024, 7, 6120−6129

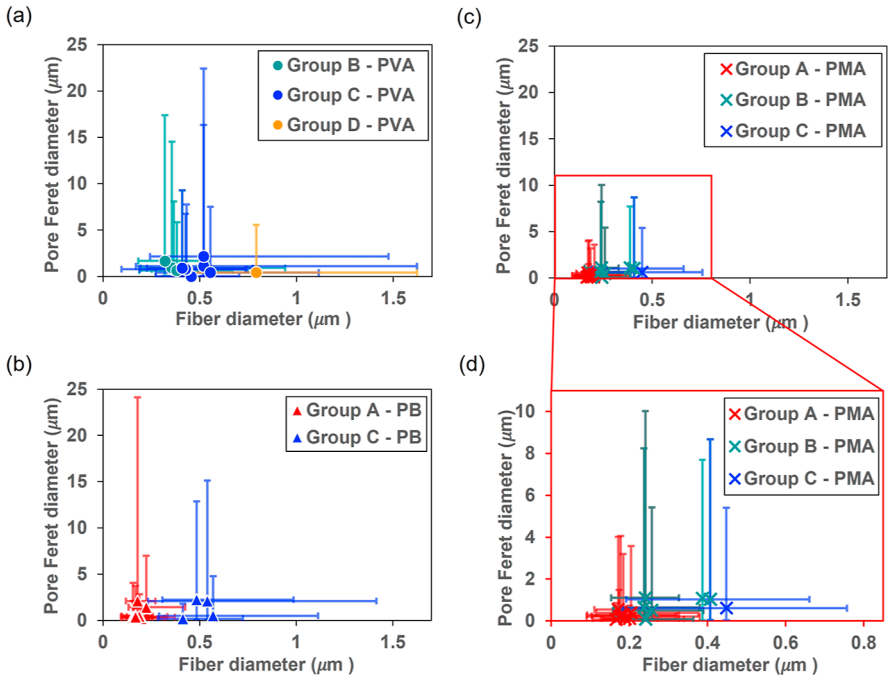

Figure 4. Pore versus fiber size distributions for (a) PVA, (b) 70/30 PVA/PB, and (c) 70/30 PVA/PMA electrospun samples [inset (d) is the expanded axis]. Mean, min, and max diameters are plotted for each individual spin sample.

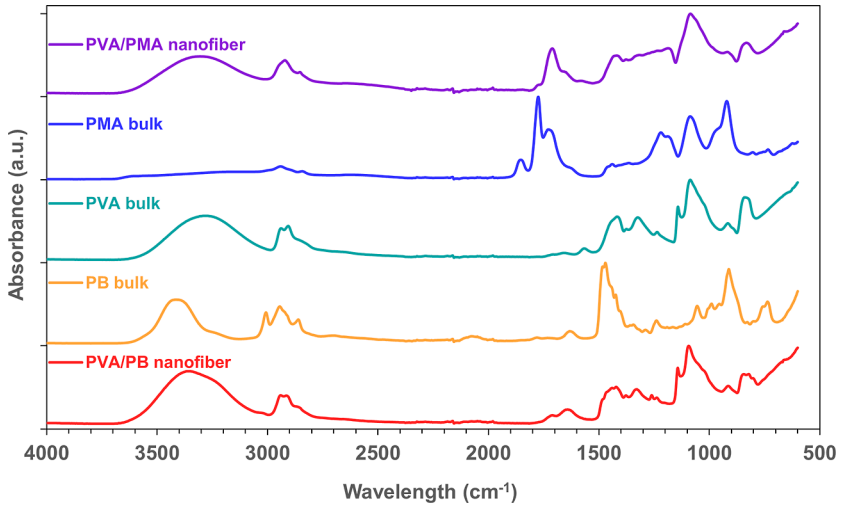

Figure 5. FTIR spectra of electrospun PVA/PMA nanofibers (purple), pure PMA polymer (blue), pure PVA polymer (green), pure PB polymer (orange), and electrospun PVA/PB nanofibers (red). Nanofiber spectra show that both PVA and the corresponding functional polymer (PMA and PB) are both present.

the hybridized fibers and successful cross-linking. Addition of PMA to PVA is confirmed by the presence of the carboxyl groups at 1720 cm^{-1} and the absence of the maleic anhydride peaks at 1853 cm^{-1} (symmetric C═O stretch, weaker peak) and 1780 cm^{-1} (asymmetric C═O stretch, stronger peak). PB is difficult to specifically identify with FTIR due to the quaternary ammonium cations lacking N−H bonds stretches, but the change in intensities and shifts in peaks in the 3100−3550 cm^{-1} region can be attributed to hydrogen bonding between PVA and PB.[25,26] EDX, as shown in Figure S6b, confirmed the presence of bromine in the PBA/PB nanofibers that is not detected in PVA and PVA/PMA in Figure S6a,c, respectively.

3.2. TENG Assembly Characterization. To demonstrate the charge dynamics of the fibers, a TENG prototype assembly with copper bottom and top plates attached to negative and positive probes and PP nonwoven layers sandwiching the electrospun layer was monitored for the change in output voltage and current from finger tapping to simulate the compression and releasing action of breathing. Output current was low (±1.05 μA) to safely come in contact with the human face, and no meaningful differences were detected between the fiber types. Figure 6 illustrates the output voltage differences between the fiber types under both dry and wet conditions.

Under dry conditions, all polymer types behaved similarly, and no hysteresis was observed. The wet condition showed differentiation between PP alone and nanofiber coatings. The control of two layers of base PP fabric alone was not able to generate charge from tapping because there is no differential in the triboelectric performance. Therefore, any electrostatic

https://doi.org/10.1021/acsanm.3c06034
ACS Appl. Nano Mater. 2024, 7, 6120−6129

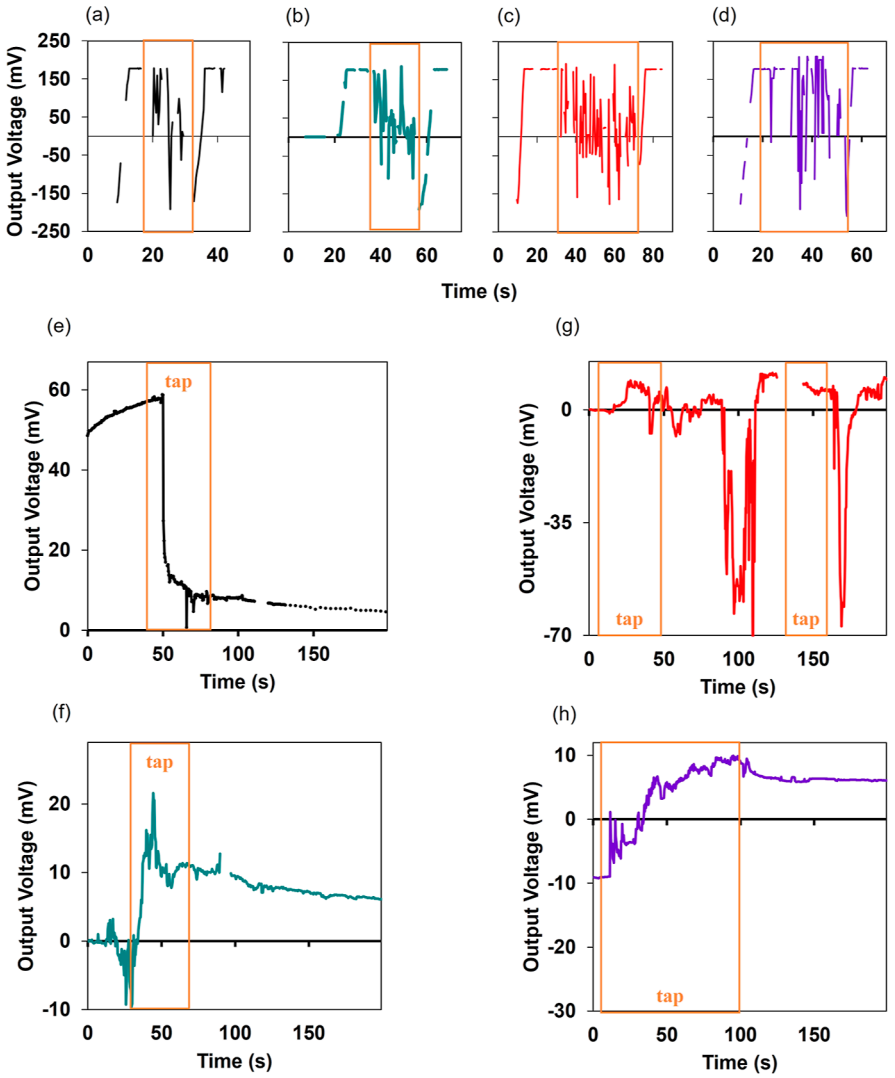

Figure 6. Output voltage (mV) of the dry condition during finger tapping and resting periods for (a) PP, (b) PVA, (c) PVA/PB, and (d) PVA/PMA. Output voltage (mV) of the wet condition response to finger tapping for € PP, (f) PVA, (g) PVA/PB, and (h) PVA/PMA.

charge that originated in the fabric or salt solution was effectively dislodged from the system by tapping, as shown by the plunge in charge during tapping and sustained charge decay after tapping stopped. All nanofiber layer samples had different triboelectric behavior than the PP substrate layers. Although direct measurement was not possible, the triboelectric nature of PVA is known to be positive; the addition of PMA is expected to make the resulting triboelectric behavior more positive, while the addition of PB would make the resulting triboelectric behavior less positive compared to PVA. However, both PMA and PB inhibited the hybrid PVA nanofibers from generating the output voltage of pure PVA nanofibers. PP, as mentioned above, has a strong negative triboelectric behavior. This presence of nanofiber layers, between the PP layers, allowed for TENG charge generation when the system was tapped, which decayed slowly after the tapping ceased. The difference in the PVA, PVA/PB, and PVA/PMA charge behaviors can be attributed to the hydrogen bonding of the water with the nanofiber surfaces and the differences in the ionic charge of the nanofiber surfaces. The Lewis acid (quaternary ammonium cation), base (carboxyl group), and free hydroxyl groups on PB, PMA, and PVA, respectively, all allow for donor−acceptor and hydrogen bonds with water. With a portion of these chemical functional groups occupied by cross-linking in the hybrid PVA nanofibers, the total available functional groups are reduced compared to pure PVA nanofibers as shown in the reduced output voltage of the hybrid PVA nanofiber samples. All samples lost charge when moisture was introduced, approximately 170 mV for stable dry conditions versus approximately −10 to 50 mV for initial wet condition. Initial charge depended on the electrolytic behavior of the ionic salt solution interacting with the polymers. For samples containing thin nanofiber layers, the charge regenerated with the mechanical action of tapping. Only the PVA/PB sample did not slowly lose voltage after tapping; instead, it rapidly dropped to approximately −70 mV before returning to the initial voltage value. This fluctuation in the voltage could be attributed to the nature of the quaternary ammonium cations. However, the control sample with two PP layers (no nanofiber layer) continued to lose charge with mechanical perturbations. These charge behavior differences from dry to wet conditions helped to elucidate the complex mechanical, moisture, and particle capture dynamics occurring during the simulated breathing tests.

3.3. Simulated Breathing. The effect of adding a thin layer of nanofiber web onto a PP microfiber substrate was

https://doi.org/10.1021/acsanm.3c06034
ACS Appl. Nano Mater. 2024, 7, 6120−6129

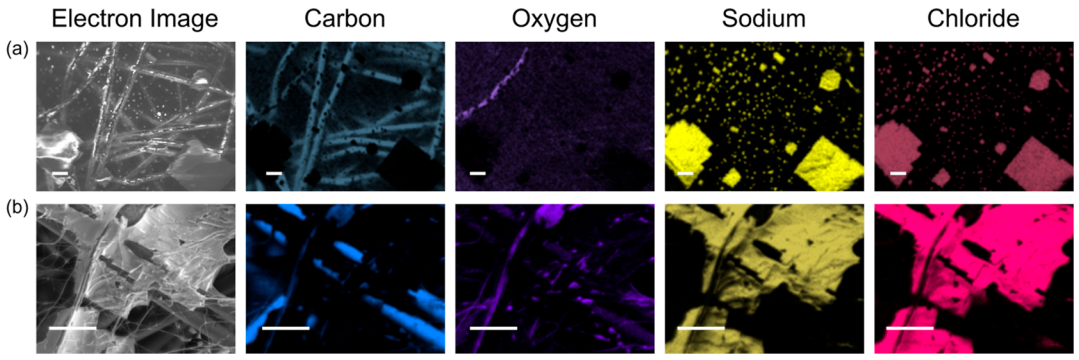

Figure 7. Elemental mapping of nanofiber morphology and salt deposition after breathing test reveals aerosol was captured as either (a) solid salt particles or (b) aqueous salt droplets. Scale bars are 50 μm.

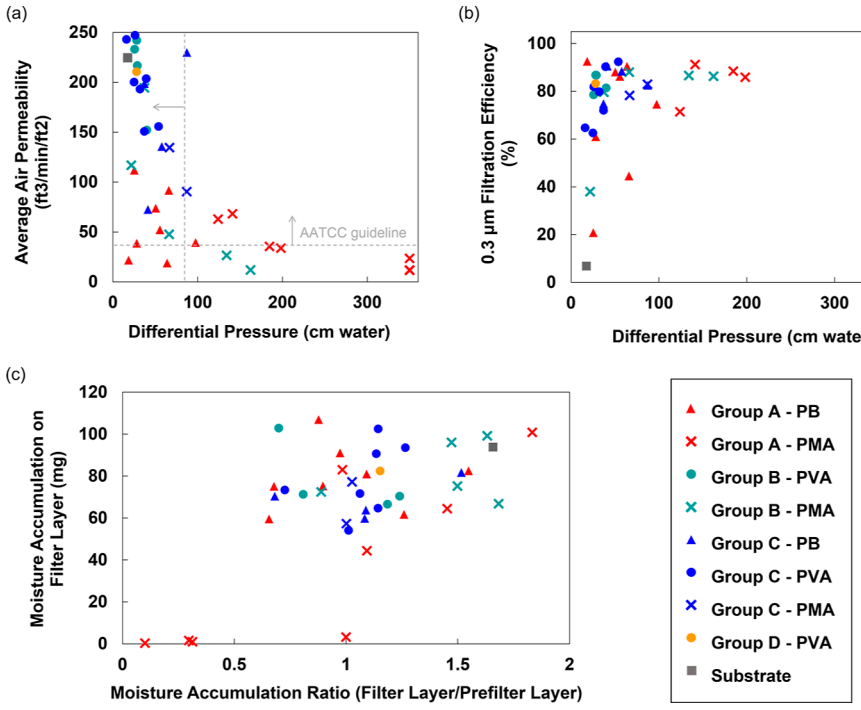

Figure 8. PVA and hybrid PVA samples during the simulated breathing were measured for (a) static (AP) versus dynamic (dP) breathability of filter assemblies, (b) 0.3 μm FE (%) versus dP (cm water) of filter assemblies, and (c) moisture accumulation (mg) on the filter layer versus the ratio of moisture accumulation on the filter layer to prefilter layer. Shared legend is bottom right.

quantified by subjecting the filter assembly to simulated breathing of sodium chloride aerosol. The PP substrate as a single layer and double layer captured a steady-state FE of −10.0 ± 0.8% and 6.8 ± 8.0% for 0.3 μm particles, 66.5 ± 6.7% and 97.8 ± 0.2% for 0.5 μm particles, and 93.5 ± 1.8% and 99.4 ± 0.4% for 1.0 μm particles. The PP as a prefilter causes some of the larger particles to break up into <0.3 μm particles (i.e., negative 0.3 μm FE) but effectively captures 0.5 and 1.0 μm particles before they reach the nanofiber layer. Therefore, all 0.3 μm capture performance in assembled PP/nanofiber/PP samples is attributed to the addition of a nanofiber web. Filter performance of the 0.3 μm particles was analyzed based on nanofiber size and composition (Table 2). The statistical design was unbalanced, since the groupings did not contain the same number of samples. Group D was not included in the statistical analysis but was used for demonstration purposes. From the remaining groups, Group C did not meet the requirements for a minimum of three samples per polymer.

3.3.1. Postbreathing Fiber Morphology and Particle Deposition Modes. Elemental mapping with EDX in Figure 7 shows that the thermally treated nanofiber webs maintain their morphology and that salt particles are deposited in two modes. That is, the nanofibers show no evidence of swelling or dissolution and solidification due to the stabilization step of the sample preparation. The nanofibers were strong enough to withstand the forces generated during simulated tidal breathing. The only fractures observed were the nanonets on PVA alone and the thinnest of the PVA/PMA fibers, but no tears were observed on larger scales.

The two modes of salt deposition observed were aqueous salt droplets and solid salt particles. The evaporation of water droplets and condensation of water vapor onto salt nuclei reach equilibrium within 1 μs after aerosol formation.[10] Particle droplets are initially formed during the pneumatic atomization and, at room temperature, will precipitate into a solid cubic crystal if the relative humidity is lower than the crystallization point.[10] Solid particles act as nuclei for water

https://doi.org/10.1021/acsanm.3c06034
ACS Appl. Nano Mater. 2024, 7, 6120−6129

vapor condensation, but this droplet formation only occurs at high saturation ratios.[10] Therefore, we consider the mixture of wet particle droplets and dry solid particles to be in equilibrium when they reach the filter sample. The droplet is larger than its crystallized salt particle but still follows the particle flow dynamics and capture mechanisms. The only difference is that once the droplet is captured, it can act as a liquid film and improve the adhesive force, and thus, capture of subsequent particles.[10] Since sodium chloride salt is used in this study, the salt particles will dissolve when they come in contact with water on the surface of the nanofibers and solidify into a filter cake when allowed to dry. Films containing only sodium and chloride (no carbon or oxygen from potentially dissolved polymers) were observed by EDX mapping on all polymer types in various thicknesses and surface areas. Evidence of solid salt particles was observed as individual salt cubes on nanofiber or substrate fiber surfaces. The salt films can inhibit air flow and increase the differential pressure, whereas the particles deposited on the fiber surface will not affect the breathability. These nanofiber webs were able to effectively capture both wet and dry particles, which represent both exhaled breath (source control) and contaminants from the environment (personal protection). While the model aerosol used here was sodium chloride salt which exhibits ionic properties in high moisture conditions, real-world particles' ionic behavior, and thus particle capture, will vary. For example, pH-dependent ionic regions in the coating of viruses affect the charge distribution and electrophoretic mobility of the virus.[31]

3.3.2. Breathability. Breathability of the filter assemblies was measured in both static and dynamic states: air permeability and in-line differential pressure (dP), respectively. The AATCC recommended AP threshold of 37.5 ft3/min/ft^2 was converted to 85.3 cm water for dP threshold based on the nominal face velocity and ratio of AP and dP sample areas. Both thresholds are displayed in Figure 8a; the optimal filters operate at high AP and low dP (top left corner of the graph). Overall, the filter assemblies followed the expected relationship between static and dynamic breathability. Samples with smaller fibers such as PVA/PMA packed tighter to create smaller pores and more tortuous path for air to flow through. The higher breathing resistance—lower AP and higher dP—would be uncomfortable or unsafe to breathe through as a face mask. PVA had larger fibers, larger pores, and looser packing, so these samples categorically had the best combination of low dP and high AP.

3.3.3. Filtration Efficiency. Each filter assembly was subjected to simulated tidal breathing at high breathing frequency for 30 min. Tidal flow is an important parameter chosen in this study to more closely replicate the real-world scenario of the mask application with a respiration-driven TENG performance. Every sample exhibited low initial FE, rapid growth over the first 5−8 min, and steady-state plateau for the last 15 min (Figure S7). The average value in the steady-state region was calculated for each size channel and is reported in Figure 8b. While these filter assemblies did increase in FE and dP over the 30 min simulated breathing, the filter cake that forms did not obstruct the airflow pathways enough to sustain a continuous growth in differential pressure. Instead, a plateau was seen in both the FE and dP, which is essential for long durations of mask use.

Nanofiber size and dP did not explain all of the variability in the FE results. That is, smaller fibers and higher dP correlate to higher FE for PMA only. As shown in Figure 8a, most of the PMA samples had the highest dP, and Figure 8b shows that the PMA sample with the highest dP captured nearly 100% of the 0.3 μm particles. This sample had a small fiber size and high packing density with small pore sizes. PB samples within the same small fiber group were capable of negligible to small increase in dP compared to substrate alone (18.3−63.8 versus 17.4 cm water), while capturing 86.3−92.5% of 0.3 μm particles. The medium and large fiber size PVA samples had minimal increase in dP but FE ranged from 62.6 to 90.3%. These comparisons suggest that the FE is not a function of the physical properties of the filter assemblies alone and that the charge output (TENG) from the tidal flow is contributing to the sustained filter performance.

The PVA and hybrid PVA nanofibers harness the moisture from the ambient environment and aerosol to maintain their adsorption capacities over the length of breathing. The prefilter layer and filter (nanofiber + substrate) layer were weighed separately before, directly after, and 24 h after the simulated breathing experiment to measure the moisture accumulation and salt capture. Between 1.6 and 21.1 mg of salt and 0.3 and 147.3 mg of water were captured by each layer (5.2−39.0 mg salt and 3.3−250.2 mg water combined total). All samples had negligible salt capture difference (<8 mg) between the prefilter and filter layers. The prefilter served to collect the fine particles, as shown with the high 0.5 and 1.0 μm FE of the single- and double-layer PP. These fine particles individually have higher mass than the ultrafine particles, but the challenge aerosol contained three magnitudes higher 0.3 μm particles by count than 1.0 μm particles. Therefore, collectively, the salt mass mostly balanced out between the particle counts and particle masses for the two layers. Moisture accumulation was more variable between and within polymer types, as shown in Figure 8c, normalized by using the ratio of filter to prefilter moisture accumulation. PMA had the widest range of accumulation ratio between filter and prefilter layers whereas PB and PVA had between 0.6 and 1.6 ratio of filter to prefilter moisture accumulation. Since the PP prefilter layer is nonwetting, the moisture accumulation is dependent on the driving force of breathing and capillary action through the layer's pores. The prefilter is therefore also dependent on the dP of the filter layer. The filter layer moisture accumulation exhibited a weak relationship to filter layer dP. Therefore, the moisture accumulation is also a function of surface chemistry (ie. hydrogen bonding and acid/base interactions with the salt water).

The cross-linking between PVA and PMA during thermal treatment reduces the amount of hydrogen bond acceptor and Lewis base sites available to interact with water and salt, respectively, therefore reducing the adsorption capacity of PMA compared to PVA and PB. Of the smaller-fiber PMA samples, the ones with the higher moisture accumulation were the ones to have lower dP and FE. The samples with the lowest moisture accumulation had the highest differential pressure and near 100% FE. The pores were too small, and the fibers were packed too densely for water droplets to pass through the filters even with the driving force of the simulated breathing. This lack of water absorption can also affect the TENG performance. Therefore, the FE for PMA is attributed to the sieve effect of the compact nanofibers and pores with a negligible surface chemistry effect. As the fiber size of PMA increased, more moisture accumulated, and more of an effect on dP was seen than FE. FE was mostly maintained, while dP

https://doi.org/10.1021/acsanm.3c06034
ACS Appl. Nano Mater. 2024, 7, 6120−6129

was lowered by 43−89%. A similar surface chemistry−water interaction effect was seen for PB and PVA. Even with larger fibers and lower dP, the FE was able to remain high with minimal web coverage. Thus, the nanofiber size ("slip"), pore size, web density, and surface chemistry contributed to the overall FE and dP.

4. CONCLUSIONS

In this study, hybrid PVA nanofibers were electrospun onto a PP nonwoven substrate, sandwiched with a PP nonwoven prefilter, and tested as self-charging, surface-active, highly efficient, and breathable filters for use in face masks. Aqueous sodium chloride was used as the challenge aerosol, and a simulated breathing apparatus was used to mimic the tidal flow of regular breathing pattern. Moisture and particle accumulation were shown to enhance the filtration performance over time without hindering the breathability. Variations in the surface chemistry of the polyionic polymers, PB and PMA, contributed to the electrospinning, fiber size properties, and output voltage generation and stability. PMA had a negligible effect on the triboelectric strength of the positive PVA, while PB decreased the triboelectric strength of PVA, particularly when moisture is introduced. Maximum 0.3 μm particle FE of 99.99% and dP of 350 cm water was achieved by the smallest fiber and pore sizes of PVA/PMA. A better balance between FE and dP was found to be 92.3% and 53.8 cm water, 92.5% and 18.3 cm water, and 88.0% and 66.1 cm water for large PVA fibers, small PVA/PB fibers, and medium PVA/PMA fibers, respectively. This study was the first step in verifying the viability of these functional nanofiber webs as general face mask filters. The surface-active PVA/PMA and PVA/PB nanofiber layers were shown to maintain filtration performance similar to that of the PVA nanofibers alone and can be used in the next step testing the nanowebs as multifunctional filters that can selectively capture and detect target pathogens (nanobugs).

■ ASSOCIATED CONTENT

Supporting Information

The Supporting Information is available free of charge at https://pubs.acs.org/doi/10.1021/acsanm.3c06034.

Additional SEM images of fiber morphology; fiber size distributions; pore size distributions; EDX spectra of nanofibers; and example of filtration efficiency versus time plot (PDF)

■ AUTHOR INFORMATION

Corresponding Author

Katarina E. Goodge − *Fiber Science Program, Department of Human Centered Design, College of Human Ecology, Cornell University, Ithaca, New York 14853, United States;* orcid.org/0000-0001-9262-4125; Email: keg222@cornell.edu

Authors

Wendy A. Alwala − *Fiber Science Program, Department of Human Centered Design, College of Human Ecology, Cornell University, Ithaca, New York 14853, United States*

Margaret W. Frey − *Fiber Science Program, Department of Human Centered Design, College of Human Ecology, Cornell University, Ithaca, New York 14853, United States;* orcid.org/0000-0003-1125-6098

Complete contact information is available at: https://pubs.acs.org/10.1021/acsanm.3c06034

Author Contributions

K.E.G.: Planned and performed experiments, analyzed data, and wrote manuscript drafts. W.A.A.: Performed experiments and aided in writing and editing the manuscript. M.W.F.: Provided guidance on the experimental design and data analysis as well as reviewed and edited the manuscript. The manuscript was written through contributions of all authors. All authors have given approval to the final version of the manuscript.

Funding

This work was supported in part by the intramural research program of the U.S. Department of Agriculture, National Institute of Food and Agriculture, and Multistate Research Project (NC-170) under grant 7003308. The findings and conclusions in this publication have not been formally disseminated by the U.S. Department of Agriculture and should not be construed to represent any agency determination or policy.

Notes

The authors declare no competing financial interest.

■ ACKNOWLEDGMENTS

This work made use of the Cornell Center for Materials Research Shared Facilities, which are supported through the NSF MRSEC program (DMR-1719875), and Department of Human Centered Design Facilities.

■ REFERENCES

(1) Viscusi, D. J.; Bergman, M.; Sinkule, E.; Shaffer, R. E. Evaluation of the Filtration Performance of 21 N95 Filtering Face Piece Respirators after Prolonged Storage. *Am. J. Infect. Control* **2009**, *37* (5), 381−386.

(2) Moyer, E. S.; Bergman, M. S. Electrostatic N-95 Respirator Filter Media Efficiency Degradation Resulting from Intermittent Sodium Chloride Aerosol Exposure. *Appl. Occup. Environ. Hyg.* **2000**, *15* (8), 600−608.

(3) Motyl, E. *Effect of Air Humidity on Charge Decay and Lifetime of PP Electret Nonwovens*; Fibres & Textiles in Eastern Europe, 2006.

(4) Lee, J.; Lee, K.; Park, H.; Kim, J. Environmental Storage Conditions Influencing the Filtration Behavior of Electret Filters with Repeated Use. *J. Ind. Text.* **2022**, *52*, 152808372211194.

(5) Lee, J.; Kim, J. Material Properties Influencing the Charge Decay of Electret Filters and Their Impact on Filtration Performance. *Polymers* **2020**, *12* (3), 721.

(6) Liao, L.; Xiao, W.; Zhao, M.; Yu, X.; Wang, H.; Wang, Q.; Chu, S.; Cui, Y. Can N95 Respirators Be Reused after Disinfection? How Many Times? *ACS Nano* **2020**, *14* (5), 6348−6356.

(7) Ullah, S.; Ullah, A.; Lee, J.; Jeong, Y.; Hashmi, M.; Zhu, C.; Joo, K. I.; Cha, H. J.; Kim, I. S. Reusability Comparison of Melt-Blown vs Nanofiber Face Mask Filters for Use in the Coronavirus Pandemic. *ACS Appl. Nano Mater.* **2020**, *3* (7), 7231−7241.

(8) Kim, J.; Hinestroza, J. P.; Jasper, W.; Barker, R. L. Effect of Solvent Exposure on the Filtration Performance of Electrostatically Charged Polypropylene Filter Media. *Text. Res. J.* **2009**, *79* (4), 343−350.

(9) Naragund, V. S.; Panda, P. K. Electrospun Nanofiber-Based Respiratory Face Masks—a Review. *Emergent Mater.* **2022**, *5* (2), 261−278.

(10) Hinds, W. C. *Aerosol Technology: Properties, Behavior, and Measurement of Airborne Particles*, 2nd ed.; Wiley: New York, 1999.

(11) Mahdavi, A.; Haghighat, F.; Bahloul, A.; Brochot, C.; Ostiguy, C. Particle Loading Time and Humidity Effects on the Efficiency of

an N95 Filtering Facepiece Respirator Model under Constant and Inhalation Cyclic Flows. *Ann. Occup. Hyg.* **2015**, *59* (5), 629−640.
(12) Łowkis, B.; Motyl, E. Electret Properties of Polypropylene Fabrics. *J. Electrost.* **2001**, *51*−*52*, 232−238.
(13) Chen, X.; Miao, L.; Guo, H.; Chen, H.; Song, Y.; Su, Z.; Zhang, H. Waterproof and Stretchable Triboelectric Nanogenerator for Biomechanical Energy Harvesting and Self-Powered Sensing. *Appl. Phys. Lett.* **2018**, *112* (20), 203902.
(14) Liu, L.; Zhou, L.; Zhang, C.; Zhao, Z.; Li, S.; Li, X.; Yin, X.; Wang, J.; Wang, Z. L. A High Humidity-Resistive Triboelectric Nanogenerator via Coupling of Dielectric Material Selection and Surface-Charge Engineering. *J. Mater. Chem. A* **2021**, *9* (37), 21357−21365.
(15) Liu, G.; Nie, J.; Han, C.; Jiang, T.; Yang, Z.; Pang, Y.; Xu, L.; Guo, T.; Bu, T.; Zhang, C.; Wang, Z. L. Self-Powered Electrostatic Adsorption Face Mask Based on a Triboelectric Nanogenerator. *ACS Appl. Mater. Interfaces* **2018**, *10* (8), 7126−7133.
(16) Wang, N.; Feng, Y.; Zheng, Y.; Zhang, L.; Feng, M.; Li, X.; Zhou, F.; Wang, D. New Hydrogen Bonding Enhanced Polyvinyl Alcohol Based Self-Charged Medical Mask with Superior Charge Retention and Moisture Resistance Performances. *Adv. Funct. Mater.* **2021**, *31* (14), 2009172.
(17) Zhang, Z.; Ji, D.; He, H.; Ramakrishna, S. Electrospun Ultrafine Fibers for Advanced Face Masks. *Mater. Sci. Eng., R* **2021**, *143*, 100594.
(18) Lu, T.; Cui, J.; Qu, Q.; Wang, Y.; Zhang, J.; Xiong, R.; Ma, W.; Huang, C. Multistructured Electrospun Nanofibers for Air Filtration: A Review. *ACS Appl. Mater. Interfaces* **2021**, *13* (20), 23293−23313.
(19) Ogbuoji, E. A.; Zaky, A. M.; Escobar, I. C. Advanced Research and Development of Face Masks and Respirators Pre and Post the Coronavirus Disease 2019 (COVID-19) Pandemic: A Critical Review. *Polymers* **2021**, *13* (12), 1998.
(20) Guerreiro, S. F. C.; Ferreira, C. A. M.; Valente, J. F. A.; Patrício, T. M. F.; Alves, N. M. F.; Dias, J. R. Electrospun-Based Membranes as a Key Tool to Prevent Respiratory Infections. *Polymers* **2022**, *14* (18), 3787.
(21) Arora, S.; Majumdar, A. Face Masks to Fight against COVID-19 Pandemics: A Comprehensive Review of Materials, Design, Technology and Product Development. *J. Ind. Text.* **2022**, *51* (3_suppl), 3613S−3647S.
(22) Deng, W.; Sun, Y.; Yao, X.; Subramanian, K.; Ling, C.; Wang, H.; Chopra, S. S.; Xu, B. B.; Wang, J.-X.; Chen, J.-F.; Wang, D.; Amancio, H.; Pramana, S.; Ye, R.; Wang, S. Masks for COVID-19. *Advanced Science* **2022**, *9* (3), 2102189.
(23) Zakrzewska, A.; Haghighat Bayan, M. A.; Nakielski, P.; Petronella, F.; De Sio, L.; Pierini, F. Nanotechnology Transition Roadmap toward Multifunctional Stimuli-Responsive Face Masks. *ACS Appl. Mater. Interfaces* **2022**, *14* (41), 46123−46144.
(24) Najafi, M.; Chery, J.; Frey, M. M. Functionalized Electrospun Poly(Vinyl Alcohol) Nanofibrous Membranes with Poly(Methyl Vinyl Ether-Alt-Maleic Anhydride) for Protein Adsorption. *Materials* **2018**, *11* (6), 1002.
(25) Cho, D.; Matlock-Colangelo, L.; Xiang, C.; Asiello, P. J.; Baeumner, A. J.; Frey, M. W. Electrospun Nanofibers for Microfluidic Analytical Systems. *Polymer* **2011**, *52* (15), 3413−3421.
(26) Xiao, M.; Chery, J.; Frey, M. W. Functionalization of Electrospun Poly(Vinyl Alcohol) (PVA) Nanofiber Membranes for Selective Chemical Capture. *ACS Appl. Nano Mater.* **2018**, *1* (2), 722−729.
(27) Matlock-Colangelo, L.; Coon, B.; Pitner, C. L.; Frey, M. W.; Baeumner, A. J. Functionalized Electrospun Poly(Vinyl Alcohol) Nanofibers for on-Chip Concentration of E. Coli Cells. *Anal. Bioanal. Chem.* **2016**, *408* (5), 1327−1334.
(28) Reyes, C. G.; Frey, M. W. Morphological Traits Essential to Electrospun and Grafted Nylon-6 Nanofiber Membranes for Capturing Submicron Simulated Exhaled Breath Aerosols. *J. Appl. Polym. Sci.* **2017**, *134* (17), 44759.
(29) Potisk, T.; Remškar, M.; Pirker, L.; Filipič, G.; Mihelič, I.; Ješelnik, M.; Čoko, U.; Ravnik, M. Single-Layer and Double-Layer Filtration Materials Based on Polyvinylidene Fluoride-Co-Hexafluoropropylene Nanofibers Coated on Melamine Microfibers. *ACS Appl. Nano Mater.* **2023**, *6* (17), 15807−15819.
(30) Lee, K.; Kim, D.; Kim, J. Computational Modeling of Multiscale Air Filter Media Consisting of Nano- and Microfibers. *ACS Appl. Nano Mater.* **2023**, *6* (11), 9415−9425.
(31) Jin, Y.; Flury, M. Fate and Transport of Viruses in Porous Media. In *Advances in Agronomy*; Sparks, D. L., Ed.; Advances in Agronomy; Academic Press, 2002; Vol. *77*, pp 39−102. .

https://doi.org/10.1021/acsanm.3c06034
ACS Appl. Nano Mater. 2024, 7, 6120−6129